AD-A175 696 SIMPLE LASER-DRIVEN METAL PHOTOCATHODES AS COLD HIGH CURRENT ELECTRON SOURCES(U) NAVAL POSTGRADUATE SCHOOL MONTEREY CA J D SAUNDERS DEC 86 1/1

UNCLASSIFIED F/G 20/5 NL

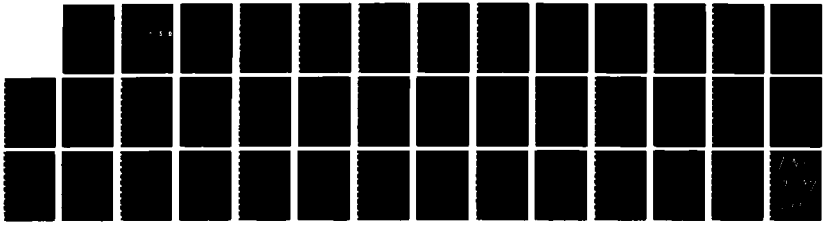

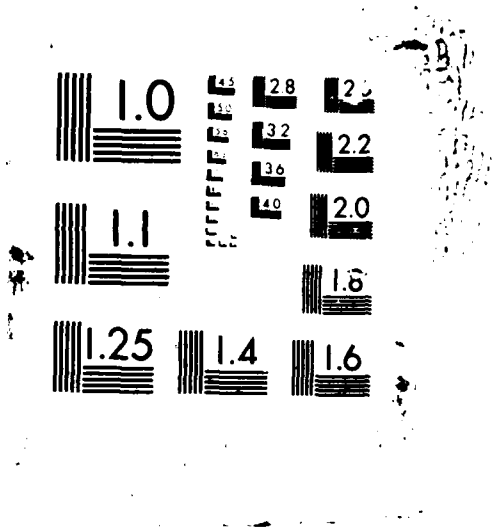
1.0
1.1
1.25
1.4
1.6
2.2
2.0
1.8

AD-A175 696

NAVAL POSTGRADUATE SCHOOL
Monterey, California

DTIC
ELECTE
JAN 05 1987
S D
D

THESIS

SIMPLE LASER-DRIVEN, METAL PHOTOCATHODES
AS
COLD, HIGH CURRENT ELECTRON SOURCES

by

Jimmy Dale Saunders

December 1986

Co-Advisor F.R. Buskirk
Co-Advisor D.C. Moir

Approved for public release; distribution is unlimited.

DTIC FILE COPY

87 1 05 012

REPORT DOCUMENTATION PAGE

1a REPORT SECURITY CLASSIFICATION UNCLASSIFIED #175 6-96	1b RESTRICTIVE MARKINGS
2a SECURITY CLASSIFICATION AUTHORITY	3 DISTRIBUTION / AVAILABILITY OF REPORT Approved for public release; distribution is unlimited.
2b DECLASSIFICATION / DOWNGRADING SCHEDULE	
4 PERFORMING ORGANIZATION REPORT NUMBER(S)	5 MONITORING ORGANIZATION REPORT NUMBER(S)
6a NAME OF PERFORMING ORGANIZATION Naval Postgraduate School 6b OFFICE SYMBOL (If applicable) 61	7a NAME OF MONITORING ORGANIZATION Naval Postgraduate School
6c ADDRESS (City, State, and ZIP Code) Monterey, CA 93943-5000	7b ADDRESS (City, State, and ZIP Code) Monterey, CA 93943-5000
8a NAME OF FUNDING / SPONSORING ORGANIZATION 8b OFFICE SYMBOL (If applicable)	9. PROCUREMENT INSTRUMENT IDENTIFICATION NUMBER
8c ADDRESS (City, State, and ZIP Code)	10 SOURCE OF FUNDING NUMBERS PROGRAM ELEMENT NO / PROJECT NO / TASK NO / WORK UNIT ACCESSION NO

11 TITLE (Include Security Classification)
SIMPLE LASER-DRIVEN, METAL PHOTOCATHODES AS COLD, HIGH CURRENT ELECTRON SOURCES

12 PERSONAL AUTHOR(S)
Saunders, Jimmy D.

13a TYPE OF REPORT	13b TIME COVERED	14 DATE OF REPORT (Year, Month, Day)	15 PAGE COUNT
Master's Thesis	FROM _____ TO _____	1986 December	39

16 SUPPLEMENTARY NOTATION

17 COSATI CODES			18 SUBJECT TERMS (Continue on reverse if necessary and identify by block number)
FIELD	GROUP	SUB-GROUP	Electron Guns Photoemissive Electron Sources KrF Laser Photoemission

19 ABSTRACT (Continue on reverse if necessary and identify by block number)

Recent developments in excimer laser design have made near ultraviolet light intensities of several megawatts per square centimeter possible in unfocused beams. These advances and recent experiments indicate that high-current, simple-metal photoemissive electron guns are now feasible. Such guns should produce greater than 50 Amps per square centimeter of illuminated cathode surface. Additionally, these guns could operate at vacuums of 10^{-6} torr with no complicated system components inside the vacuum enclosure. The electron beam produced by such photoemission guns would have a very low emittance and high brightness. This beam would also follow closely the temporal characteristics of the laser pulse, making fast risetime, ultra-short electron beam pulses possible.

20 DISTRIBUTION / AVAILABILITY OF ABSTRACT	21 ABSTRACT SECURITY CLASSIFICATION
☒ UNCLASSIFIED/UNLIMITED ☐ SAME AS RPT ☐ DTIC USERS	UNCLASSIFIED
22a NAME OF RESPONSIBLE INDIVIDUAL Prof. F. R. Buskirk	22b TELEPHONE (Include Area Code) 408-646-2765 22c OFFICE SYMBOL 61Bs

DD FORM 1473, 84 MAR 83 APR edition may be used until exhausted
All other editions are obsolete

Approved for public release; distribution is unlimited.

Simple Laser-Driven, Metal Photocathodes
as
Cold, High Current Electron Sources

by

Jimmy Dale Saunders
Lieutenant Commander, United States Navy
B.S., University of Mississippi, 1976

Submitted in partial fulfillment of the
requirements for the degree of

MASTER OF SCIENCE IN PHYSICS

from the

NAVAL POSTGRADUATE SCHOOL
December 1986

Author: Jimmy Dale Saunders
Jimmy Dale Saunders

Approved by: Fred R Buskirk
F.R. Buskirk, Co-Advisor

D.C. Moir, Co-Advisor

Gordon E. Schacher, Chairman,
Department of Physics

John N. Dyer,
Dean of Science and Engineering

ABSTRACT

Recent developments in excimer laser design have made near ultraviolet light intensities of several megawatts per square centimeter possible in unfocused beams. These advances and recent experiments indicate that high-current, simple-metal photoemissive electron guns are now feasible. Such guns should produce greater than 50 Amps per square centimeter of illuminated cathode surface. Additionally, these guns could operate at vacuums of 10^{-6} torr with no complicated system components inside the vacuum enclosure. The electron beam produced by such photoemission guns would have a very low emittance and high brightness. This beam would also follow closely the temporal characteristics of the laser pulse, making fast risetime, ultra-short electron beam pulses possible.

Accesion For	
NTIS CRA&I	☒
DTIC TAB	☐
Unannounced	☐
Justification	
By	
Distribution /	
Availability Codes	
Dist	Avail and / or Special
A-1	

TABLE OF CONTENTS

LIST OF TABLES

LIST OF FIGURES

ACKNOWLEDGEMENTS

The experiments conducted as the basis for this thesis were supported by the Hydrodaynamics Group, Los Alamos National Laboratory. Technical support and guidance was primarily provided by Doctor D.C. Moir and Doctor S.W. Downey of the Beam Dynamics Section. The direction and support from both were invaluable. Doctor Downey is currently with AT&T Bell Labs.

I wish to give special recognition to Judy Saunders of the Naval Postgraduate School. Her procedural and formatting expertise greatly contributed to the correct and timely submission of this paper.

I. INTRODUCTION

High-current particle accelerators require sophisticated engineering and manufacturing techniques. Electron gun engineering and construction is particularily challenging. Frabrication of the emitting cathode is difficult and for current photoemissive cathodes requires in situ preparation at high vacuum (10^{-10} torr). Some emitting cathodes are subject to frequent maintenance and replacement. Thermionic and field emission electron guns require a complicated and expensive pulse power source. In addition, desirable fast rise time pulses are difficult to achieve due to the intrinsic character of the pulsed power supplies used in thermionic and field emission guns.

Recent developments in pulsed excimer lasers have made possible ultraviolet (UV) photon intensities of several megawatts per square centimeter in unfocused beams. These UV laser advances beg a review of previous photoemission studies and new experiments designed to ascertain the feasibility of improving electron gun beam quality and design while reducing the complexity of the gun system. Such a review is in progress at Los Alamos National Laboratory where the experiments described in this paper were conducted.

A. HISTORICAL BACKGROUND

In experiments concluded in 1887 Heinrich Hertz discovered that spark discharge occured more easily between two electrodes when one was illuminated by ultraviolet light [Ref. 1]. After the discovery of the electron, Philipp Lenard concluded by 1902 that this effect was due to electron emission by the illuminated metal, and further that there was a minimum frequency of the light below which no electron emission was observed [Ref. 2,3]. Contemporary theories could not explain this observation until Albert Einstein advanced his Nobel Prize winning "photoelectric law" in 1905. He contended that light was radiated and absorbed in energy quanta [Ref. 4]. Einstein postulated that the maximum kinetic energy ($\mathbf{E}_{k\,m}$) of the emitted electron was Plank's constant ($\hbar$) times the light frequency (ν) minus "Austrittsarbeit" (φ), the emission work or work function [Ref. 5: p. 3], as shown in Equation 1.1 ,

$$\mathbf{E}_{km} = \hbar\nu - \varphi. \tag{1.1}$$

The elegance of Einstein's theory failed to sway the bulk of the scientific community, and it was not until 1916, when Robert Millikan carefully measured the kinetic energy of electrons liberated by different frequencies of light, that his theory gained universal acceptance [Ref. 6].

Subsequently, much effort was expended in obtaining work functions for various metals, but the values acquired varied widely due to ill defined surface conditions [Ref. 5: p. 3]. The discovery in 1923 by Kingdon and Langmuir that cesium coatings lowered the work function of tungsten sparked new enthusiasm in photoemission [Ref. 7]. It was found that alkali metal coatings could produce electron per photon yields on the order of one in ten [Ref. 8]. Since the 1940's most photoemission study effort has been centered around the alkali metals, efficiencies of 10% are lucrative compared to 0.001% for more commonly known simple metals [Ref. 9].

B. PHOTOEMISSIVE ELECTRON GUNS

High-current electron guns of the thermionic, field and photoemissive types are currently operational. However, both the thermionic and field emitting guns suffer from the temporal pulse limitations of the pulsed power sources and have difficulty maintaining a high operating tempo. Current photoemissive guns use alkali metal coated cathodes and produce currents as high as 200 A cm^{-2} in a 1 cm^2 beam cross section [Ref. 10]. The reactivity of the alkali metal cathodes dictate a vacuum near 10^{-10} torr. In addition, the cathode must be manufactured and transfered in high vacuum, which can be a lengthly process, and it must be conditioned in the gun.

By contrast, simple-metal photocathode electron guns do not exist in operational accelerators. However, today's "off the shelf" excimer lasers provide enough intensity to overcome the poor quantum yields of simple metals. If sufficient current could be obtained from such a gun, the resulting beam would be temporally consistent with the laser pulse, making fast rise times and ultrashort pulses possible. Additionally, the transverse kinetic energy of the beam electrons should be less than the work function of the metal, providing excellent emittance and brightness. Another advantage of the simple-metal cathode gun would be the ability to operate without the need to enter the vacuum enclosure for gun maintenance. All complicated system components would function outside the vacuum boundary. Such a gun would function in a moderate vacuum, 10^{-6} torr, and thus avoid many problems routinely associated with ultra-high vacuum systems.

C. OBJECTIVES

This paper presents the results of recent laboratory experiments conducted on a simple-metal photocathode electron gun. The results should provide some measure of the practical feasibility of such a gun for use in a high-current particle accelerator. The parameter estimates considered necessary to make a judgement of feasibility are presented in this paper and are listed below:

1. Current density
2. Total current
3. Emittance and brightness
4. Practical quantum yield.

Since the experimental apparatus and diagnostic methods were not highly sophisticated, it is recognized that the margin of error in some parameters may be significant. However, the purpose of the experiments is to gauge the possibilities of simple-metal cathode photoemissive guns and assess the direction and focus of the next generation experimental investigation.

II. THEORETICAL CONSIDERATIONS

A theoretical description of the photoemission process is no simple challenge. Such a model must deal with many properties of the material, among which are the ground and excited state atomic electron structure, the static and driving electromagnetic fields, surface contaminates, lattice orientation, and the radical changes of medium across the vacuum interface. The difficult experimental problems, due to surface condition and lattice orientation, reduced most early empirically obtained parameters such as work function to rough estimates. Advances in solid state theory have added much to our understanding, but a comprehensive photoemission model has yet to be validated. Current and past theories are particularly inadequate in addressing the simple, non-alkali metals. [Ref. 11]

No attempt is made to qualify or validate any existing theoretical model of photoemission. However, the so called "three step process" is reviewed to establish a basis for the remaining discussion. A theoretical treatment of various models may be found in *Photoemission and the Electronic Properties of Surfaces* (1978) [Ref. 12].

A. PHOTOEMISSION, A THREE STEP PROCESS

The liberation of electrons from a material is considered either a surface effect or a volume effect, or both, by various theorists in the field. The degree of correlation between theory and empirical data varies with the wavelength of the incident light, the material illuminated, surface contaminates, lattice orientations, polarization of incident light and other factors. The mechanisms involved in this complicated process can be better understood if broken down into stages. A convenient and accepted method is to divide the process into three events, which are photon absorption, electron motion and electron surface barrier penetration [Ref. 13].

1. Photon Absorption

For simple metals a significant portion of the incident photon flux will be reflected. The surface characteristics are, of course, important since contamination, impurities and surface roughness will all effect the reflectivity of the surface. Additionally, near surface conditions such as vacuum level and plasma formation could cause screening of incident photons. The remaining photons penetrate the material to depths of more than 100 Å for ultra violet wavelengths [Ref. 5: p. 2], being primarily lost to quanta absorption by electrons.

Einsteins's orginal expression (Eqn. 1.1) can be modified to account for the entire spectrum of excited electron energies. Only the maximum kinetic energy is considered in the usual expression, where as all energy states are accounted for in Equation 2.1.

$$E_k = \hbar\nu - \varphi - E_i, \tag{2.1}$$

where E_i is the initial electronic energy state of a given electron. The kinetic energy (E_k) of the electron is the photon energy ($h\nu$) minus the work function (φ) minus the initial electronic energy state below the Fermi level (E_f) [Ref. 14]. By limiting the photon energy to just above the target's work function, a pictorial representation of the expected emitted electron energy spectra can be devised, see Figure 2.1.

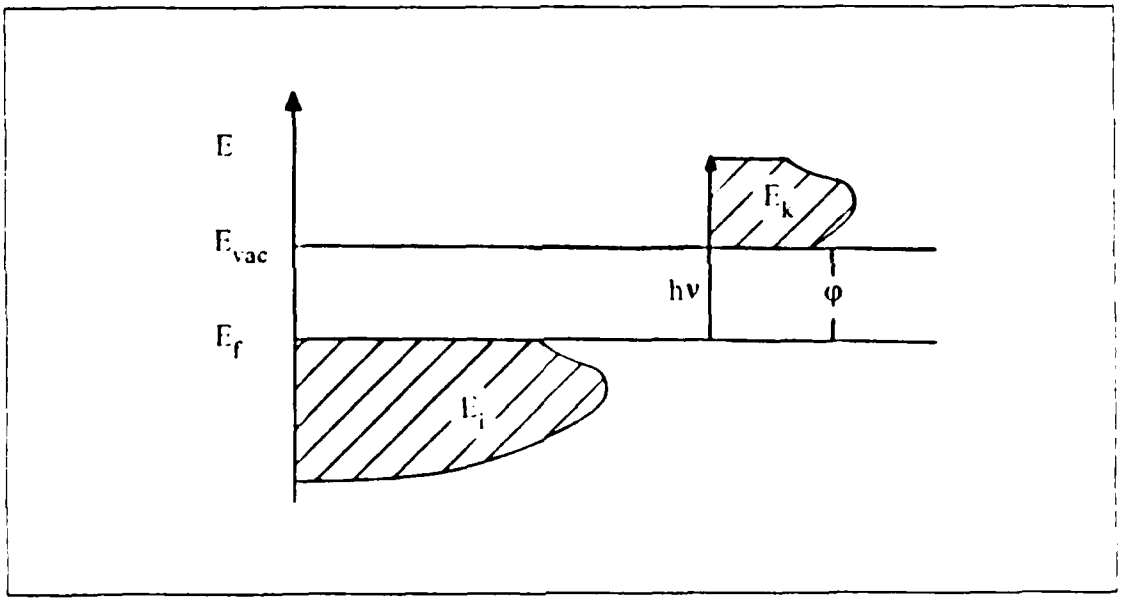

Figure 2.1 Electron Energy Distribution.

This simple interpretation also allows envisioning surface effects, properties unique to those electrons excited near the surface. The energy spectra can be modified by treating the initial and final state wavefunctions local to the surface. Thus allowing the initial and final state functions to be different for the surface than for the bulk material. Surface properties may result in modification of the expected spectral distribution due to plasmon interaction. Additionally, an electron liberated from the

interior must have a momentum component normal to the surface that corresponds to sufficient kinetic energy, hence velocty, to overcome the work function of the metal. By contrast, an electron emitted near the surface need not meet these criteria if any surface roughness exsists. In other words, plasmon energy may be imparted to the electron helping it to overcome the surface barrier. In addition, the required momentum component normal to the surface for electron escape may be smaller than expected if escape directions other than normal to the surface are possible.

In summary, the above description predicts an incident photon flux diluted by reflection, and contaminate and plasma screening effects. The remaining flux penetrates to depths of about one hundred lattice layers. These photons produce a spectrum of free electron energy states in the material or at the surface. The observable part of this spectrum lies above the vacuum energy of the material. [Ref. 12: pp. 7-8]

2. Electron Motion

The photoexcited electrons are at higher energies than the bulk free electrons in the metal. Hence, the excited electrons will undergo scattering processes until each escapes the material or reaches thermal equilibrium. In metals the large number of free electrons dictates that electron-electron scattering will be the dominant loss mechanism. The large number of electron collisions suffered by the photoexcited electrons causes the range over which energy is lost to be very small. For maximum energies of 5 eV, the distance is about 4 A, which corresponds to about two lattice layers [Ref. 5: p. 2]. Thus, only electrons excited very near the surface have a reasonable probability of reaching the vacuum interface. Since most electrons are excited at depths of many lattice layers and most excited electrons reaching the surface are produced only a few lattice layers deep, the quantum efficiency, which is the ratio of the number of emitted electrons to the number of absorbed photons, is very small. This fact coupled with the expected spectral contributions of surface properties produces a complex distribution of electron energies at the surface of the metal. [Ref. 15: pp. 6-7]

3. Surface Barrier Penetration

As illustrated by Figure 2.1, electrons can only escape the metal surface if they have a surface-normal kinetic energy that is greater than the work function. Most simple non-alkali metals have work functions between 4 and 5 eV. The concept of the

work function barrier is complicated by the fact that φ is a function of lattice orientation, varying in many cases by more than 10% for various orientations [Ref. 5: p. 38]. In addition, external electric fields applied to the surface lower the work function. This is known as the Schottky Effect [Ref. 16]. It operates such that φ is lowered as the square root of increasing external field (F),

$$\Delta\varphi = -(qF/4\pi\varepsilon_o)^{1/2}, \tag{2.2}$$

where q is the electron charge in coulombs, F the field in volts per meter and ε_o the permittivity in MKS units. However, local microscopic fields may be much higher than the general applied field if sharp surface irregularities are present. For a point protruding from the surface, the micro-field (F_m) is given by Equation 2.3.

$$F_m = (2V)/(r\ln(R/r)), \tag{2.3}$$

where (V) is the potential in volts, R the distance from the point to the anode and r the radius of curvature of the tip. Then, as a first approximation, the function is reduced by

$$\Delta\varphi \propto (V/r)^{1/2}. \tag{2.4}$$

A rougher surface would have smaller values of r and more protrusions. A rough surface will then generally widen and smooth the features in the spectral distribution of emitted electrons and increase the total current emitted. [Ref. 5: pp. 20-21]

B. PRACTICAL ASSUMPTIONS

If an electron gun system operates in particular situations, various aspects of the emission theory may be emphasized or neglected. The system used operates at 10^{-6} torr with applied fields of less than 10^5 V cm^{-1}. The laser light source produces 5 eV photons and illuminates the target with about 1 MW cm^{-2} of power. In addition, cathode surfaces are assumed to have roughness features of approximately 10 μm height. Given these parameters, some simplifying assumptions may be considered:

1. The moderate vacuum dictates the formation of contaminate monolayers in about one second or less [Ref. 15: p. 15]. Elaborate surface cleaning of the cathode prior to operation is useless.
2. Microfield enhancement may occur at 10^5 V cm^{-1} of applied field due to surface roughness. If "whiskers" of material protrude, some field emission might occur.
3. Since the photon energy is near the work function value of the cathode material, the average emitted electron kinetic energy is expected to be less than the work function and distributed preferencially in a direction normal to the surface.
4. The surface irregularities are many times larger than the lattice spacing. Additionally, the cathode materials are not single crystals. Hence, lattice orientation is of little consequence to the total emission.
5. The 5 eV photon penetration depth is at least of the order of the surface roughness. Thus, the entire microscopic surface is subject to electron emission.
6. The 1 MW cm^{-2} UV light power incident on the surface is not enough to cause near surface plasma formation [Ref. 17: p. 346].

III. EXPERIMENTAL TECHNIQUES

An excimer laser was used to illuminate a flat simple-metal cathode in a vacuum chamber with intense UV radiation. A positive potential was applied to the cathode to accelerate the liberated electrons toward a parallel anode plate. A conducting charge collector was located behind a small hole in the anode and its output monitored. Data were obtained by correlating the laser pulse to the output collector current for a given applied potential.

A. OPTICAL ARRANGEMENT

A Questec Model 2000 excimer laser operating in KrF (krypton-fluorine) was the radiation source. The KrF excimer laser produces a 248 nm wavelength, a photon energy of 5.0 eV, with a full pulse width of 30 ns. The laser light path components are depicted in Figure 3.1.

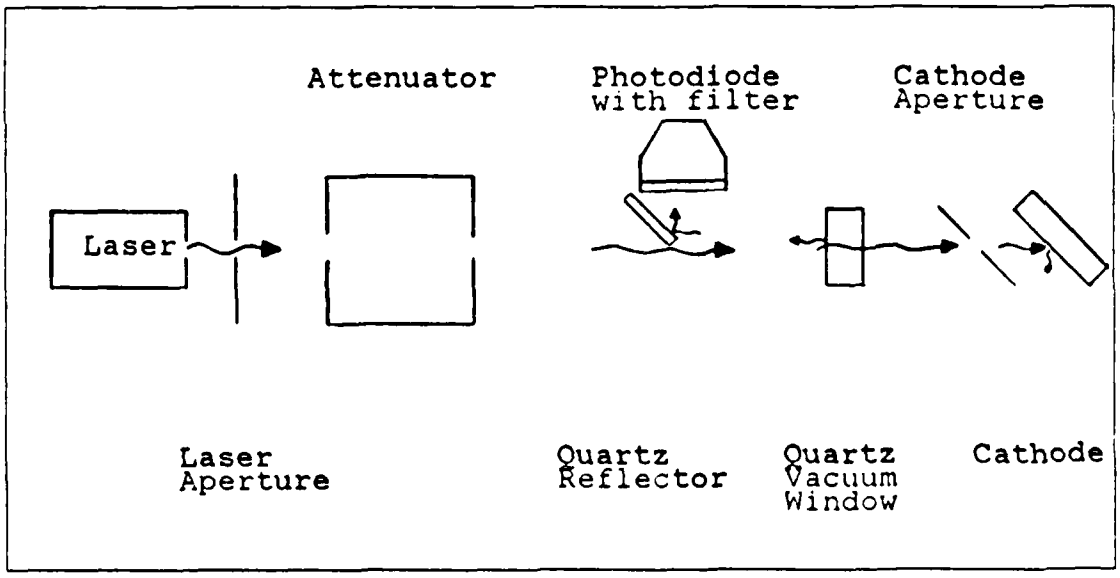

Figure 3.1 Optical Arrangement of Experiment.

Laser light at about 100 millijoules (mJ) per pulse in a 3 cm^2 beam cross section was apertured to 0.4 cm^2 and then passed through a Laser Variable Attenuator, NRC Model 935-10. The attenuated beam then passed into the vacuum chamber through a

Suprasil quartz window with the normal 8% reflection loss. The beam was again apertured (to 0.18 cm^2) and then allowed to illuminate the cathode at a 45° incident angle. Concurrently, the reflected beam from the quartz vacuum window was reflected by a 248 nm 98% reflector through a 248 nm filter onto a fast response photodiode, a Hamamatsu R1193U-04. The photodiode was used to monitor the laser beam pulse.

B. ANODE/CATHODE ARRANGEMENT

A removable metal cathode disc, 2.5 cm in diameter and 0.4 cm thick, was attached to a high-voltage connector which penetrated the vacuum chamber wall. Prior to installation the cathode was polished in air to a surface roughness of about 10 μm. When in place the cathode was centered in front of, and parallel to the anode which is of the same diameter and made of aluminum. The physical anode-cathode arrangement is illustrated in Figure 3.2.

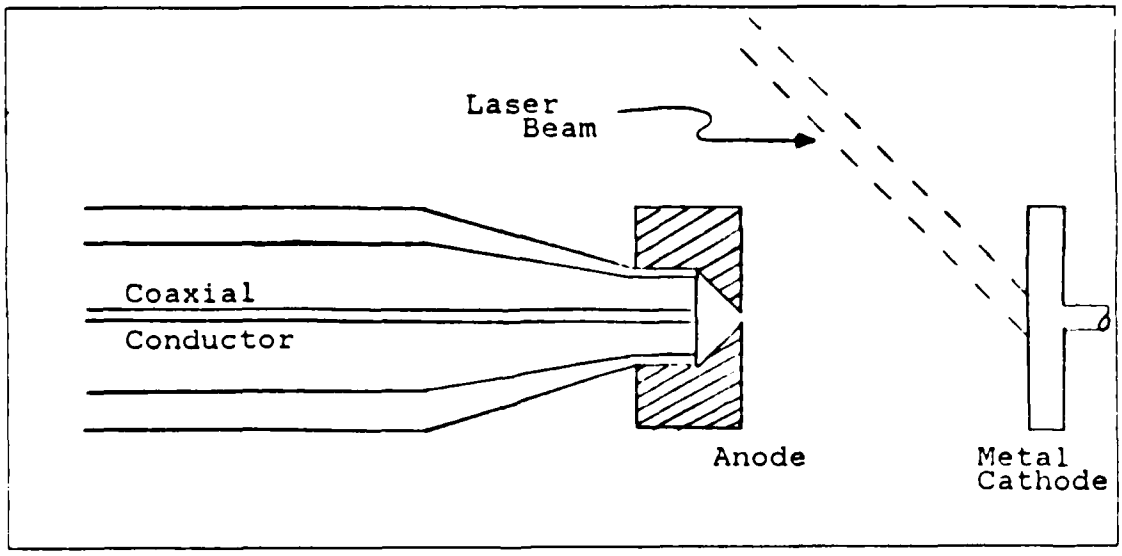

Figure 3.2 Anode-Cathode Arrangement.

The A-K gap was about 18 mm and the accelerating potential across the gap was variable from 0 to 30 kV. Electrons emitted from the 0.18 cm^2 illumination spot were accelerated toward the anode and some passed through the 0.071 cm^2 opening at the center of the anode. These electrons were then collected on an aluminum wire collector which ran parallel to the electron beam axis. The collector with a cross sectional area of 0.156 cm^2 was the center conductor of a 50 Ω coaxial cable. The

anode and all other portions of the vacuum chamber and support hardware were at ground potential. The electron pulse collected was then monitored by an oscilliscope and boxcar averager.

C. ELECTRONICS SETUP

Three electronic parameters were monitored during data acquisition:

1. The fast photodiode output voltage pulse, used to calculate laser power applied to the cathode
2. The accelerating potential, which permitted field calculations
3. The collector output voltage pulse, facillitating the collector current determination.

A wiring schematic of the monitoring equipment is shown in Figure 3.3.

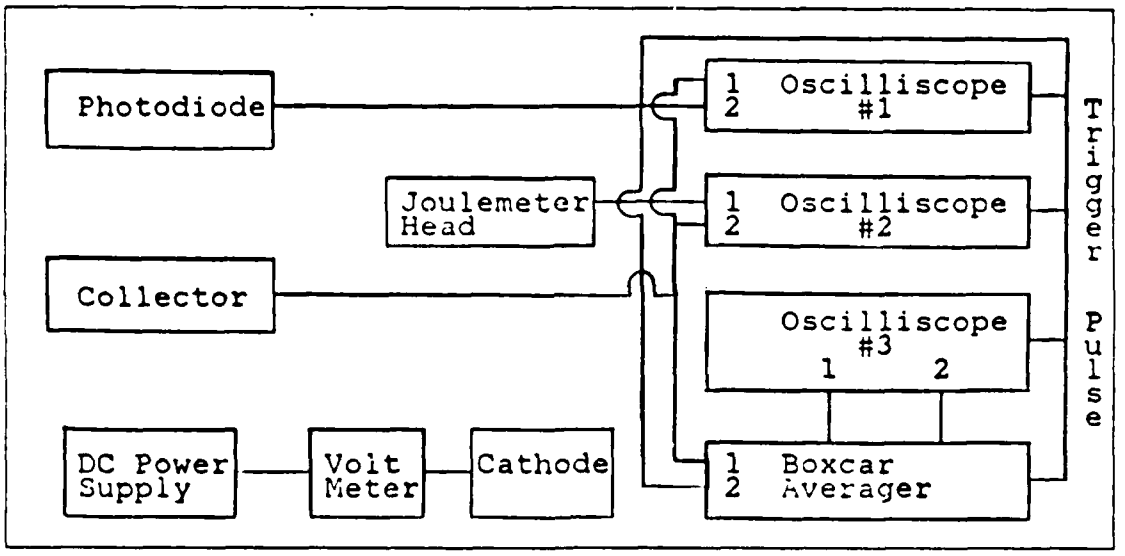

Figure 3.3 Electronic Equipment Arrangement.

The photodiode driven by the reflected laser light was used as the trigger source for all analyzing equipment. One oscilliscope was dedicated to monitoring this pulse. The second oscilliscope was used as the collector voltage monitor or the calibrating joulemeter monitor as appropriate. The third oscilliscope was used to verify proper gate to pulse alignment of the boxcar averager, an EG & G Model 162. All oscilliscopes were fast response Techtronics R-7103's. Data acquisition was primarily by oscilliscope photographs with the boxcar averager as a secondary source, the laser repetition rate used was not optimum for boxcar accuracy.

D. VACUUM SYSTEM

The vacuum system consisted of a vacuum chamber with a volume of approximately 10 liters. This chamber was sealed by neopreme o-rings and pumped by a Cryogenics Cryo-Torr-8. The best vacuum achieved was 8×10^{-8} torr after 12 hours of pumping. Most data was taken with a vacuum of about 10^{-6} torr. Since the nature of the experiment required frequent adjustments inside the vacuum chamber with no remote manipulation ability, the vacuum boundary was frequently broken.

IV. DATA ACQUISITION AND REDUCTION TECHNIQUES

The general technique for obtaining data was simple. A photon beam pulse was attenuated as desired and illuminated the cathode. Electrons liberated from the cathode were accelerated toward the anode. Some of these electrons passed through a hole in the center of the anode and struck the end of the collector wire. A portion of the photon pulse was reflected and measured giving laser power. The collector current pulse was also measured and then compared to the laser power.

Three experimental apparatus limitations affected the range and accuracy of the data. The accelerating potential electrical connection to the cathode was rated at 25 kV standoff and could not be relied upon to hold off breakdown above 28 kV. In addition, the minimum anode-cathode gap achievable was 1.8 cm, resulting in a maximum field of less than 15 kV cm^{-1}. Secondly, the current collector electronic system had an inherent noise level which tended to chop and distort the current pulse signal for collector currents below about 0.7 mA. But most significantly the laser power used was low and did not facillitate direct energy measurement of individual laser pulses, and short pulse duration (30 ns) did not lend itself well to temporal measurements by joulemeters. The energy of the system was diagnosed using a fast response photodiode calibrated in the system relative to a Gentec-200 calorimeter nead.

A. LASER PULSE ENERGY DIAGNOSTIC

The fast photodiode output was highly non-linear as a function of the pulse energy. Comparison between photodiode output voltage and joulemeter values showed the energy to vary approximately as the sixth power of the photodiode voltage. A photodiode output voltage (V) to joulemeter energy (E) calibration curve was obtained just prior to data acquisition. The data taken was found to fit the relation shown in Equation 4.1.

$$E = 0.0046V^{6.16}, \tag{4.1}$$

where V is the photodiode output voltage in volts and E is the pulse energy in mJ.

Although the oscilliscope measurement of the photodiode voltage was accurate to within 2%, the high power of V in Equation 4.1 made the corresponding error in E

very large. Hence, an approximate error of 15% is attributed to this source. There existed a 1 to 5% error in joulemeter readings coupled with calorimeter head calibration accuracy of 10%. Overall a 15% error is attributed to the joulemeter. The total error of 30% was somewhat diminished by averaging 20 successive pulses to obtain each value used. A calibration curve error margin of 10% is consequently assumed.

B. CURRENT MEASUREMENT DIAGNOSTIC

The collector voltage was measured to within 2% at high current and to within 5% at low currents. However, electronic noise within the circuit prevented accuracies of better than 10% error for currents below 0.7 mA. The system impedance (50Ω) was assumed to be accurate to within 2% and the anode collector hole area measured to within 1% of its true value. Therefore, the current measurement accuracy is assumed to be 20% error below 0.7 mA (10 mA cm^{-2}), and less than 10% error at higher currents.

Due to the low fields applied to the cathode, the current was often limited by the screening effects of the electrons released at the beginning of the pulse. The current density is limited according to the 1.5 power of the potential [Ref. 18]. The relationship is shown in Equation 4.2 .

$$J = PV^{1.5}d^{-2}, \tag{4.2}$$

where J is the current density (A cm^{-2}), d the A-K spacing (cm), V the potential (V) and P the perveance of a planar geometry (2.34×10^{-6} $AV^{-1.5}$) [Ref. 19]. This space-charge limited electron flow was an important upper bound on the data taken while determining quantum yields. In assessing the space-charge parameters, the A-K potential was measured from the calibrated meter on the power supply and was assumed to have an accuracy of 2%, 400 volts, at 20 kV. The A-K spacing was measured accurately to within 0.5 mm, an error of 3%. Since the space-charged current limit varies as the 1.5 power of the potential, the aggregate maximum expected error is 10%.

C. REFLECTANCE MEASUREMENTS

The reflectance of the cathode material was considered in arriving at actual quantum yields. The experimental values were obtained using a Gentec-500

calorimeter head monitored by an oscilliscope. The measurement is assumed to have a maximum error of 5% with a 10% calorimeter head calibration error. Thus an overall reflectance accuracy of 15% is assumed.

Consequently, the absolute quantum efficiency values are within only about 35% of the true values. However, the relative values of quantum efficiency are expected to be accurate to within 10% for the various sample cathodes.

V. RESULTS AND CONCLUSIONS

During experiments conducted to investigate the feasibility of high-current simple-metal photocathode electron guns, several cathode characteristics were measured for various materials. Quantities measured were:

1. Empirical values of reflectance for Ni, Sn, Cu, Zn, Al and Pb
2. Electric field effects on the quantum yield of Zn
3. Electron beam emittance and brightness from a ZN cathode
4. Quantum efficiencies of 5 eV photons for Ni, Sn, Cu, Zn, Al and Pb
5. Maximum current per unit area at 12 kV cm^{-1} electric field for Ni, Sn, Cu, Zn, Al and Pb.

A. REFLECTANCE

The degree of reflectance is of no practical importance unless the system is limited by the maximum power output of the laser. But, the reflected radiation could illuminate areas of the electron gun structure and cause photoemission and corresponding undesirable electromagnetic effects. This is an engineering problem with numerous possible solutions. However, if absoulte quantum efficiency calculations are desired, the reflectance must be estimated. When available optical constant values for metals were used to calculate the 45° incident reflectance of a 248 nm unpolarized laser beam [Ref. 20]. No suitable information at the proper wave length could be found for Zn, Sn, or Pb. Calculated values of reflectance for Ni, Cu and Al are listed in Table 1 for comparison with measured practical reflectance values.

Reflectance values for all examined metals were found by measuring incident and reflected energy from the cathode material with a 248 nm excimer laser UV light source at an intensity of about 1 MW cm^{-2}. The experiment was conducted with cathode surface preparation identical to that conducted prior to current measuring experiments. These practical values of reflectance ($\pm$ 15%) are also shown in Table 1. The large variation between theoretical and practical values is probably due to surface roughness and oxide layers.

TABLE 1

REFLECTANCE VALUES

Element Symbol	Theoretical Reflectance (%)	Practical Reflectance (%)
Ni	45.7	13.9
Sn	-	10.0
Zn	-	34.8
Cu	36.9	16.2
Al	64.2	42.0
Pb	-	7.2

B. FIELD EFFECTS

The investigation of the effect of the field strength on photoemission was conducted expecting that the Schottky Effect would be verified, but that was not the case. Data obtained at two different laser intensities with varying electric field strength applied to a Zn cathode is depicted in Figure 5.1. Three observations on the data are noteworthy:

1. As expected the low field data is limited by the Child-Langmuir space-charge flow limit.
2. The quantum yield does not increase as the applied electric field increases as the Schottky Effect predicts. The quantum yield and current peak in the low field region and then peak again at about 13 kV/cm, with the high field portion of the curve apparently approaching some lower constant value.
3. Increasing the laser intensity by a factor of two increased the quantum yield and shifted the peaks to higher field values.

The second and third points are not understood. Increasing quantum yield with laser power is discussed in the quantum efficiency section. The peaking phenomenon may be the result of resonant coupling with surface plasmons. But, there is no theoretical justification for such a hypothesis.

C. BEAM EMITTANCE AND BRIGHTNESS

An estimate of beam emittance was made by replacing the anode fixture with one which employed two parallel flat disc plates with a coincident collector window in each.

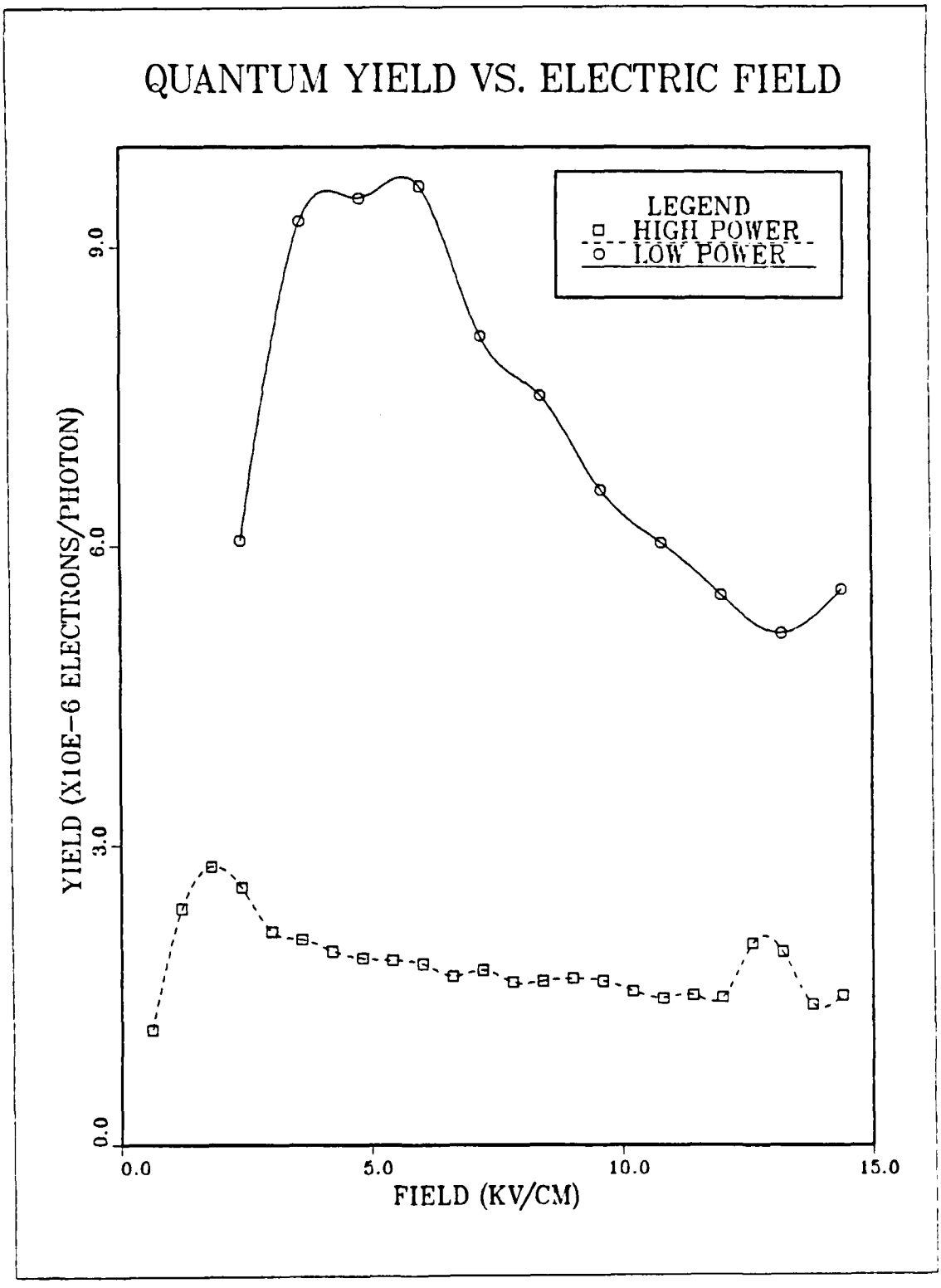

Figure 5.1 Field Effects on Quantum Efficiency.

The disc to disc spacing was 2.5 times the window diameter (0.457 mm). The experiment was operated with an accelerating potential of 20 kV and a Zn cathode. The spacing from the collector to the back of the anode was varied to obtain information on beam divergence. The calculations were made using accepted standards for normalized emittance and brightness [Ref. 21]. Four data repetitions were taken for each beam drift distance, the averages of which are given in Table 2 .

TABLE 2
EMITTANCE DATA

Drift Distance (mm)	Normalized Current (mA)	Relative Current	Beam Radius (mm)
1.060	10.90	1.000	0.457
2.117	10.70	0.979	0.462
3.175	9.63	0.881	0.487
4.233	8.79	0.804	0.510
5.292	8.23	0.753	0.527
6.350	7.73	0.707	0.543
7.408	7.44	0.680	0.554
*19.236	*5.45	*0.500	*0.646

*extrapolated

1. **Emittance**

The emittance was calculated using the extrapolated distance at which 50% of the electron beam would be uncollected by a collector with the same diameter as the initial beam. The beam is assumed to be uniform in the plane transverse to the beam axis. The extrapolated 50% loss drift distance (d) corresponds to a beam radius (r) at d. The initial beam radius (b), is then used to approximate the solid angle (α) of the beam as it diverges beyond the anode window. The approximation takes the form of Equation 5.1.

$$\alpha \sim 2 \sin^{-1}\{(r-b)\, d\}, \qquad (5.1)$$

where α is the solid angle. Substitution of the Table 2 values into Equation 5.1 yields, $\alpha = 19.7$ mrad. The emittance is defined as the solid angle (α) times the original beam radius (b), as in Equation 5.2.

$$\varepsilon = b\alpha \qquad (5.2)$$
$$= 8.98 \text{ mrad mm.}$$

The normalized emittance (ε_n) is the emittance times the relativistic particle parameters γ and β. In this case $\beta = 0.280$ and $\gamma = 1.042$. The normalized emittance can then be calculated by Equation 5.3,

$$\varepsilon_n = \beta\gamma\varepsilon \qquad (5.3)$$
$$= 0.83\pi \text{ mrad mm.}$$

This corresponds to a transverse beam temperature of 2.2 eV and is considered the maximum electron temperature in the beam. The electrons in the beam would have an equivalent temperature of 2.5×10^4 K ($\pm$ 25%).

2. **Brightness**

By assuming the electron beam to be radially and rotationally symmetric the brightness can be approximated by Equation 5.4.

$$B_n = (2I)/(\pi^2 \varepsilon_n^2), \qquad (5.4)$$

where B_n is the normalized brightness and I the total beam current in amps. By inserting the values already obtained, $B_n = 3.2 \times 10^8$ A rad^2 m^2 ($\pm$ 100%) [Ref. 21: p. 187].

D. QUANTUM EFFICIENCY

The experimental apparatus was limited by the inability to measure very low currents or obtain large fields. Within this context the various metal cathodes were examined. Each had a slightly different anode-cathode gap, and to allow for comparison, the space-charge limited data was normalized to equivalent A-K spacing. The zinc cathode used in other experiments will be presented in detail and the remaining metals presented later for comparison.

1. **Power vs. Current**

The Zn data for power versus current is displayed in Figure 5.2. Immediately observed from Figure 5.2 is that the current is not a linear function of power. In fact, well clear of the space-charge limit the curve shows current to be a quadratic function

of power. This result will be discussed in detail in the quantum yield section. Another observation is that the maximum current is well correlated to the 2.135 A cm^{-2} predicted for space-charge limited flow between parallel plates. All other metals showed similiar results, with the exception of Al which will be discussed separately.

2. **Power vs. Quantum Yield**

The practical quantum yield Zn is plotted in Figure 5.3. Again the curve near the space-charge limit behaves as expected. The low power end of the curve shows a nearly constant quantum yield. This was the predicted result, but the connecting section of the curve exhibits nearly quadratic behavior. Three possible explanations are suggested:

1. The curve shows a second order effect. As the leading edge of the pulse pumps the distribution of populated energy states toward a more excited level, the remaining pulse contributes by photon-electron interactions. These interactions provide the necessary additional kinetic energy to facillitate emission of an electron which might otherwise not penetrate the surface barrier. This two photon effect could be a volume process or could be coupled to some surface effect.
2. The curve indicates that a contaminate layer screens the photons and retards the sensed current. At higher photon intensities, the contaminates are boiled off the surface and the effect reduced.
3. The curve could indicate that the low power end of the curve is the constant quantum yield of the contaminate layers. As the power increases, these contaminates boil off and produce a surface plasma which then interacts with liberated electrons to amplify the emission current. This would suggest that higher light intensities could result in much higher quantum yields. But, the effect would be vacuum dependent and produce an increasingly poor emittance value as the power were increased.

A review of the data for other metals shows Ni the least productive with a practical quantum yield of 5.9×10^{-6} electrons per photon and Pb the most efficient with a quantum yield of 1.3×10^{-4} electrons per photon. However, both reached the space charge limit as the laser power was increased prior to the full developement of the curve which is expected to result in a constant quantum efficiency. Therefore, significantly higher yields may be possible.

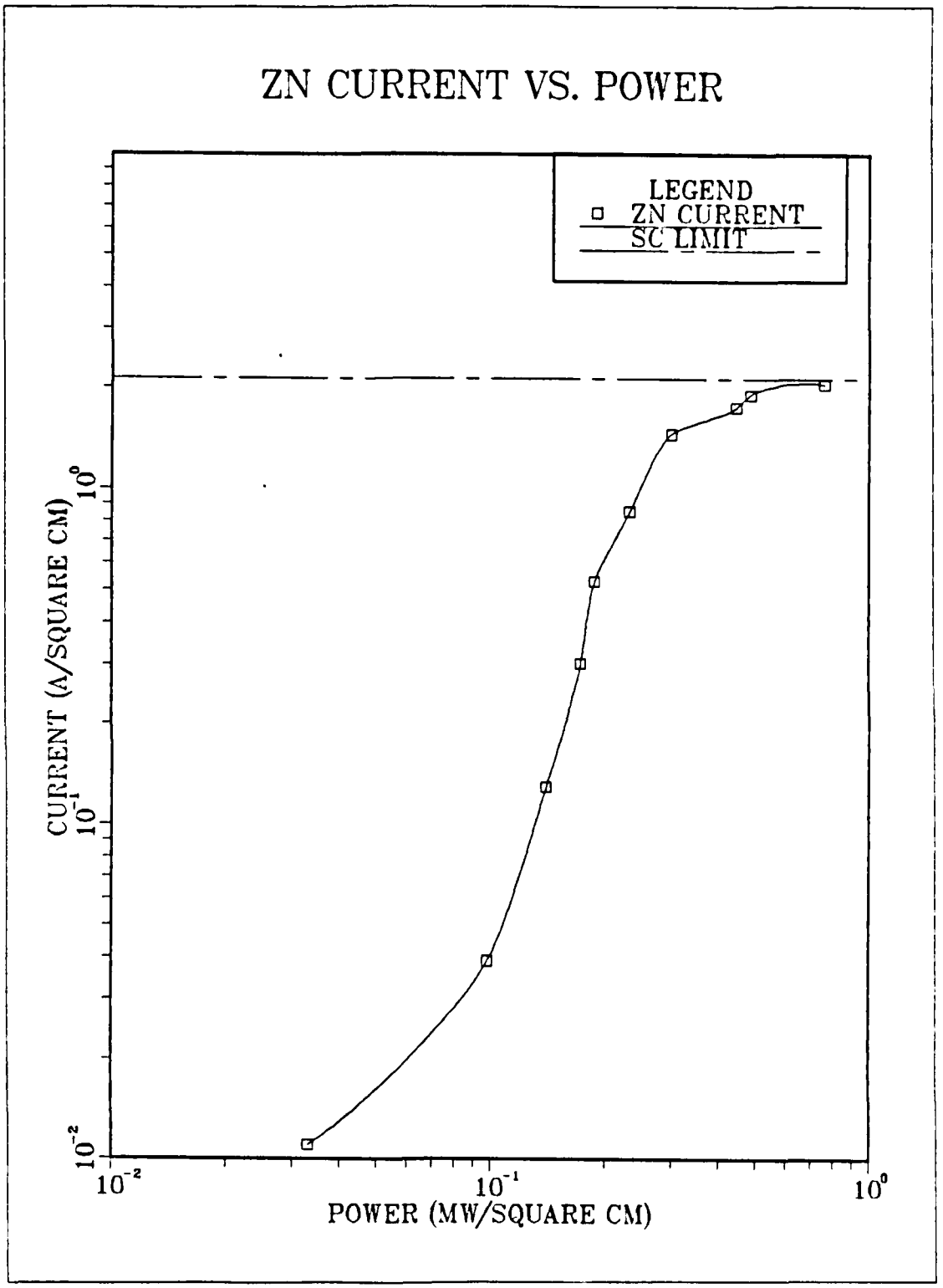

Figure 5.2 Zn Current Production.

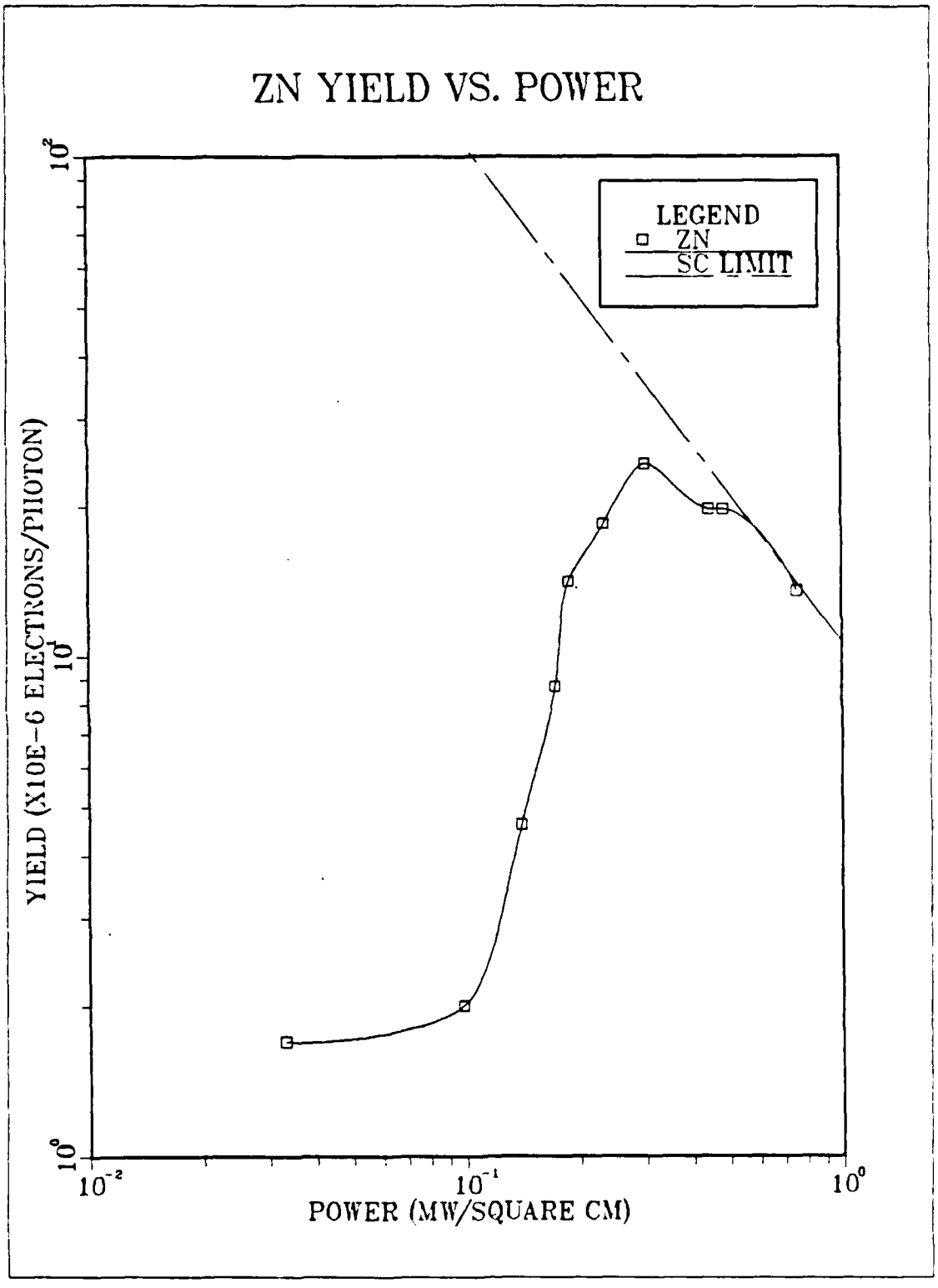

Figure 5.3 Zn Quantum Efficiency.

In the case of Al, a near constant quantum yield was obtained from 0.03 to 0.5 MW cm^{-2}. The cutoff at 0.5 MW cm^{-2} was due to the space-charge limit. Perhaps the low power end of the aluminum curve is the contaminated surface constant quantum yield. As power increases, the contaminates are burned away without sufficient time to reform before the next laser pulse. (Data was taken at a repetition rate of 3 hz). At higher powers, the surface was laser cleaned and the constant quantum yield of the Al metal was realized. If this scenerio is correct, other metals might have such a cleaning threshold which would result in much higher quantum yields than previously seen. Data for Ni, Sn and Cu is shown in Figure 5.4. Data for Zn, Al and Pb is contained in Figure 5.5.

E. EXPECTED BEAM PARAMETERS

In summary, the simple-metal photocathode electron gun operating at 10^{-6} torr and 1 MW cm^{-2} of 248 nm light intensity and at fields of only 12 kV cm^{-1} produced current densities of more than 1 A cm^{-2} in emission limit and more than 2 A cm^{-2} in space-charge limited flow. A current density of greater than 50 A cm^{-2} can be expected from a Zn cathode with higher fields but below the field emission region. Current densities higher than 70 A cm^{-2} have already been obtained from Cu cathodes at 193 nm wavelength and with a 100 kV cm^{-1} field strength [Ref. 22]. If plasma creation and surface damage do not occur until the intensity is more than 5 MW cm^{-2} as suggested by F. Schwirzke, in *Laser Interaction and Related Plasma Phenomena* (1984) [Ref. 17: p. 346], then the incident laser power could be increased by a factor of 5 over that used to obtain this data. If the near quadratic dependence of quantum yield (η) on power holds, quantum efficiencies of greater than 3×10^{-3} electrons per photon might be achieved. However, even at the quantum efficiency established here, a 5 MW cm^{-2} intensity of 248 nm photons could produce more than 23 A cm^{-2} from Zn, Al or Cu. In addition, that same current density can be produced from Pb at 1 MW cm^{-2}. A 5 cm^2 cathode could be expected to produce a beam current of 120 to 350 A, driven by an "off the shelf" KrF excimer laser. The resulting beam is expected to be very "cold", have a very low emittance, and produce sub-nanosecond rise times with easily tailored pulse lengths.

F. CONCLUSION

A high-current simple-metal photocathode is feasible. Beam current of more than 50 A cm^{-2} in a cold, high brightness regime is possible. The electron gun can

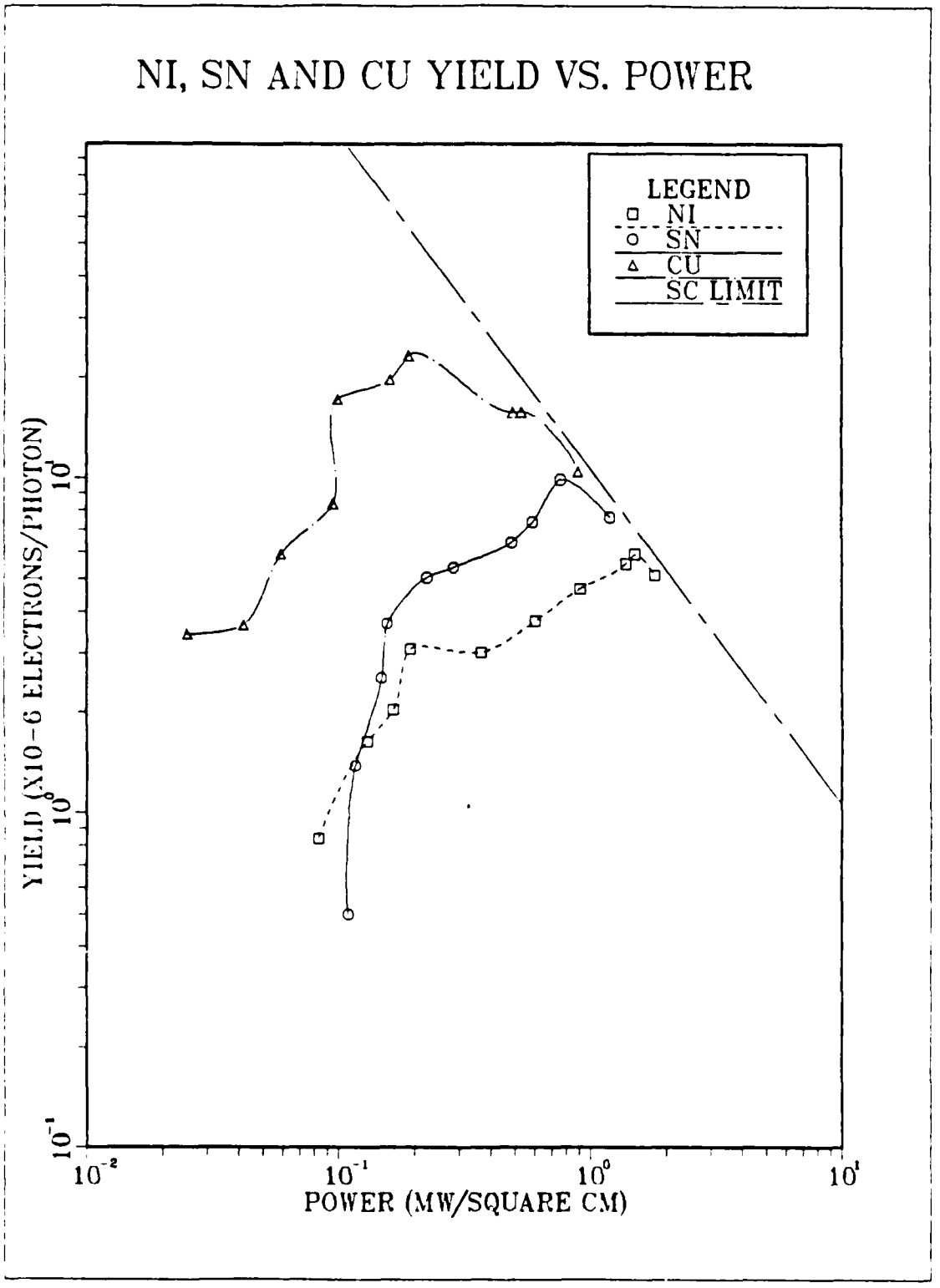

Figure 5.4 Ni, Sn and Cu Quantum Yields.

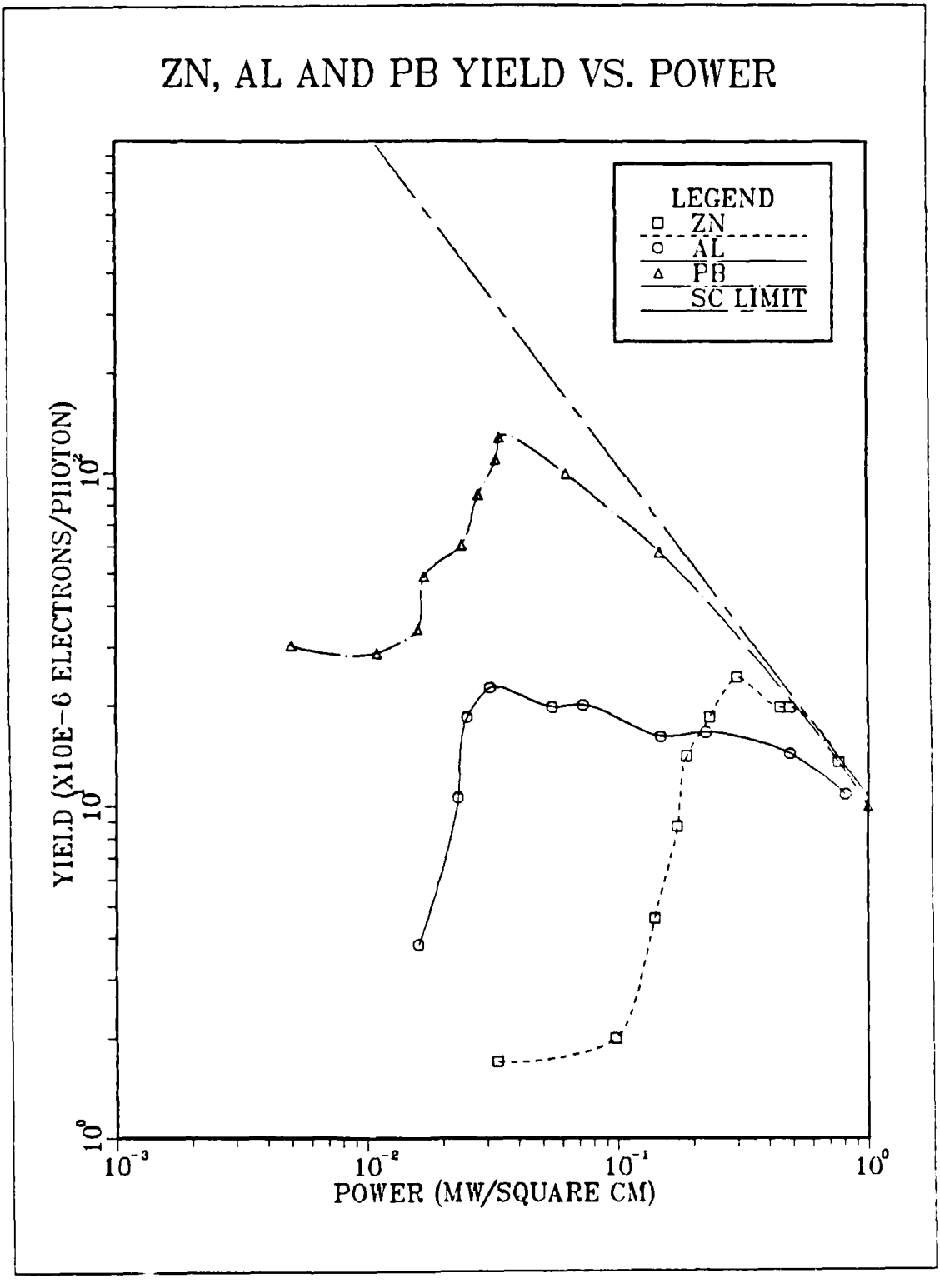

Figure 5.5 Zn, Al and Pb Quantum Yields.

operate at 10^{-6} torr and should require little maintenance inside the vacuum boundary. In addition, the temporal control over the pulse could produce extremely short, fast rise-time pulse.

Future efforts should move in the following directions:

1. Using a Pierce type electron gun design [Ref. 23], take data for metals of interest at high accelerating potentials and to low currents in order to map out the metal response curves over a wider range to verify a self-cleaning intensity level.
2. Conduct experiments using a uranium cathode due to its low work function.
3. Obtain a more precise beam mapping so that accurate values of emittance and brightness can be attained.
4. Verify the laser intensity threshold for laser damage plasma production.

LIST OF REFERENCES

1. H. Hertz, Ann. Physik **31**, 983 (1887).

2. P. Lenard, Ann. Physik **2**, 359 (1900).

3. P. Lenard, Ann. Physik **8**, 149 (1902).

4. A. Einstein, Ann. Physik **17**, 132 (1905).

5. M. Cordona and L. Ley, *Photoemission in Solids I: General Principles*, in Topics in Applied Physics, v. 26, (Springer-Verlag, N.Y., 1978) Chap. 1.

6. R.A. Millikan, Phys. Rev. **7**, 355 (1916).

7. K.H. Kingdon and I. Langmuir, Phys. Rev. **21**, 380 (1923).

8. P. Görlich, Z. Physik **101**, 335 (1936).

9. W. Krolikowski and W.E. Spicer, Phys. Rev. **185**, no. 3, 882 (1969).

10. C.H. Lee, P.E. Ottinger, E.R. Pugh, R. Klinkowstein, J.H. Jacob, J.S. Fraser and R.L. Sheffield, IEEE Trans. Nucl. Sci. **NS-32**, 3045 (1985).

11. W.L. Schaich, "Theory of Photoemission : Independent Particle Model", in *Photoemission in Solids I : General Principles*, ed. by M. Cardona and L. Ley, Topics in Applied Physics, v. 26, (Springer-Verlag, N.Y., 1978) Chap. 2.

12. N.W. Ashcroft, et. al., *Photoemission and the Electronic Properties of Surfaces*, ed. by B. Feuerbacher, B. Fitton and R.F. Willis, (John Wiley and Sons, N.Y., 1978).

13. C.N. Berglund and W.E. Spicer, Phys. Rev. **136**, A1030 (1964).

14. C. Kittel and H. Kroemer, *Thermal Physics*, 2nd ed., (W.H. Freeman and Company, N.Y., 1980), p. 155.

15. A.H. Sommer, *Photoemissive Materials: Preparation, Properties, and Uses*, (John Wiley and Sons, N.Y., 1968).

16. W. Schottky, Ann. Physik **44**, 1011 (1914).

17. F. Schwirzke, "Laser Induced Unipolar Arcing", in *Laser Interaction and Related Plasma Phenomena*, v. 6, ed. by H. Hora and G.H. Miley (Plenum Publishing Corp., N.Y., 1984).

18. I. Langmuir, Phys. Rev. **2**, ser. 2, 450 (1913).

19. J.D. Lawson, *The Physics of Charged Particle Beams*, (Oxford University, England, 1978), Chap. 3.

20. *Handbook of Optical Constants of Solids*, ed. by E.D. Palik, (Academic Press, Inc., N.Y., 1985).

21. C. LeJeune and J. Aubert, "Emittance and Brightness: Definitions and Measurements", trans. by P.W. Hawkes, *Advances in Electronics and Electron Physics: Supplement 13A*, ed. by A. Septier, (Academic Press, Inc., N.Y., 1980), pp. 176-189.

22. S.W. Downey, L.A. Builta, D.C. Moir, T.J. Ringler and J.D. Saunders, Appl. Phys. Lett. **49**, 15 (1986).

23. J.R. Pierce, *Theory and Design of Electron Beams*, (D. Van Nostrand Company, Inc., N.Y., 1954).

INITIAL DISTRIBUTION LIST

		No. Copies
1.	Defense Technical Information Center Cameron Station Alexandria, Virginia 22304-6145	2
2.	Library, Code 0142 Naval Postgraduate School Monterey, California 93943-5002	2
3.	Dr. S.W. Downey Rm 1A-352 AT&T Bell Labs 600 Mountain Avenue Murray Hill, New Jersey 07974	1
4.	Dr. D.C. Moir M-4 P940 Los Alamos National Laboratory Los Alamos, New Mexico 87545	2
5.	Lieutenant Commander J.D. Saunders, USN 585A Sampson Lane Monterey, California 93940	6
6.	Lieutenant Commander T.J. Ringler, USN 337 Tuxford Place Fayetteville, North Carolina 28303	1
7.	Mr. James H. Saunders Rt. 1 Blackwell, Texas 79506	1
8.	Mr. K.E. Falconer 907 Kenwood Lane Longview, Texas 75604	1
9.	Director Strategic Systems Project Office Attention CAPT P. Huber Washington, District of Columbia 20376-5002	1
10.	Commander Space and Naval Warfare Systems Command PMW-145A Attention CDR W.F. Bassett Washington, District of Columbia 20363-5100	1
11.	Dr. F.R. Buskirk, Code 61Bs Naval Postgraduate School Monterey, California 93943-5000	3

END

2-87

DTIC